

The earliest bird-line archosaurs and the assembly of the dinosaur body plan

Sterling J. Nesbitt¹, Richard J. Butler², Martín D. Ezcurra^{2,3}, Paul M. Barrett⁴, Michelle R. Stocker¹, Kenneth D. Angielczyk⁵, Roger M. H. Smith^{6,7}, Christian A. Sidor⁸, Grzegorz Niedźwiedzki⁹, Andrey G. Sennikov^{10,11} & Alan J. Charig⁴‡

The relationship between dinosaurs and other reptiles is well established^{1–4}, but the sequence of acquisition of dinosaurian features has been obscured by the scarcity of fossils with transitional morphologies. The closest extinct relatives of dinosaurs either have highly derived morphologies^{5–7} or are known from poorly preserved^{8,9} or incomplete material^{10,11}. Here we describe one of the stratigraphically lowest and phylogenetically earliest members of the avian stem lineage (Avemetatarsalia), *Teleocrater rhadinus* gen. et sp. nov., from the Middle Triassic epoch. The anatomy of *T. rhadinus* provides key information that unites several enigmatic taxa from across Pangaea into a previously unrecognized clade, Aphanosauria. This clade is the sister taxon of Ornithodira (pterosaurs and birds) and shortens the ghost lineage inferred at the base of Avemetatarsalia. We demonstrate that several anatomical features long thought to characterize Dinosauria and dinosauriforms evolved much earlier, soon after the bird–crocodylian split, and that the earliest avemetatarsalians retained the crocodylian-like ankle morphology and hindlimb proportions of stem archosaurs and early pseudosuchians. Early avemetatarsalians were substantially more species-rich, widely geographically distributed and morphologically diverse than previously recognized. Moreover, several early dinosauromorphs that were previously used as models to understand dinosaur origins may represent specialized forms rather than the ancestral avemetatarsalian morphology.

Birds and crocodylians, which are each other's closest living relatives and form the clade Archosauria, diverged in the Triassic period^{2,3}. The divergence of stem-avians (Avemetatarsalia) from stem-crocodylians (Pseudosuchia) is a major transition in terrestrial vertebrate evolution, involving changes in limb proportions and body size, numerous morphological innovations in the hindlimb, and, eventually, extensive forelimb modification in dinosaurs^{2,12–14}. However, those changes are poorly documented because of limited fossil records, especially for the Middle Triassic. For example, the earliest diverging group of currently known stem-avians, the pterosaurs, were already highly specialized by the time of their first appearance in the Late Triassic, providing few clues about sequences of character evolution in early stem-avians. Other key early diverging stem-avian taxa are known only from limited postcranial remains (for example, lagerpetids^{10,15}). Therefore, a clear morphological gap currently exists between dinosaurs, pterosaurs and stem-crocodylians.

Here, we name and describe, to our knowledge, the oldest member of the avian stem lineage from the lower strata of the Middle Triassic Manda Beds of Tanzania (Fig. 1). This taxon substantially enhances our knowledge of the origins and early evolution of the stem-avian

anatomical features that are characteristic of dinosaurs, while also revealing a previously undocumented combination of morphologies retained from the common ancestor of birds and crocodylians.

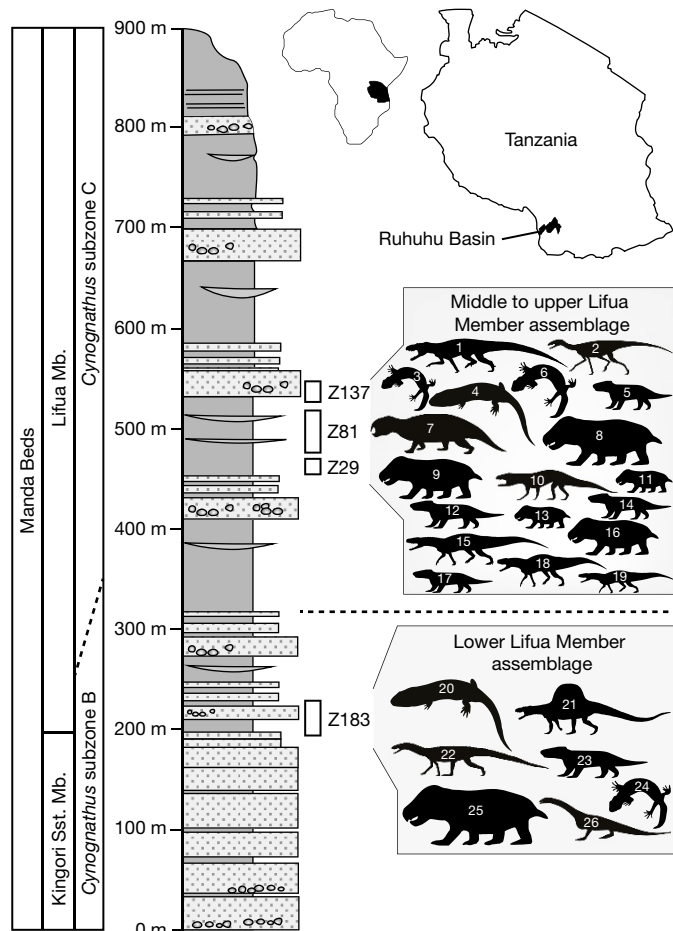


Figure 1 | Geographical and stratigraphical occurrence of *Teleocrater rhadinus* gen. et sp. nov. from the Ruhuhu Basin, southern Tanzania, Africa. Numbered silhouettes refer to taxa with specimens that are described in Supplementary Information 4. *Nyasasaurus parringtoni* is not included because its stratigraphic position is not clear. See Methods for silhouette sources. Z numbers refer to localities. Mb., Member; Sst., Sandstone.

¹Department of Geosciences, Virginia Tech, Blacksburg, Virginia 24061, USA. ²School of Geography, Earth and Environmental Sciences, University of Birmingham, Edgbaston, Birmingham B15 2TT, UK. ³CONICET—Sección Paleontología de Vertebrados, Museo Argentino de Ciencias Naturales, Buenos Aires, Argentina. ⁴Department of Earth Sciences, Natural History Museum, Cromwell Road, London SW7 5BD, UK. ⁵Integrative Research Center, Field Museum of Natural History, 1400 South Lake Shore Drive, Chicago, Illinois 60605, USA. ⁶Evolutionary Studies Institute, University of the Witwatersrand, PO Wits 2050, Johannesburg, South Africa. ⁷Iziko South African Museum, PO Box 61, Cape Town, South Africa. ⁸Burke Museum and Department of Biology, University of Washington, Seattle, Washington 98195, USA. ⁹Department of Organismal Biology, Uppsala University, Norbyvägen 18A, 752 36 Uppsala, Sweden. ¹⁰Borissiak Paleontological Institute, Russian Academy of Sciences, Profsoyuznaya 123, Moscow 117997, Russia. ¹¹Kazan Federal University, Kremlyovskaya ul. 18, Kazan 420008, Russia. [‡]Deceased.

Archosauria Cope, 1869 *sensu* Gauthier and Padian, 1985

Aemetatarsalia Benton, 1999

Aphanosauria clade nov. (see Methods)

Teleocrater rhadinus gen. et sp. nov.

Etymology. ‘Teleos’, finished or complete (Greek) and ‘krater’, bowl or basin (Greek), referring to the closed acetabulum; ‘rhadinos’, slender (Greek), referring to the slender body plan.

Holotype. NHMUK (Natural History Museum, London, UK) PV R6795, a disassociated skeleton of one individual, including: cervical, trunk, and caudal vertebrae, partial pectoral and pelvic girdles, partial forelimb and hindlimbs (Fig. 2a, d, g–k, m, o and Supplementary Tables 1, 2).

Referred material. Elements found near the holotype, but from other individuals, which represent most of the skeleton and that are derived from a paucispecific bone bed containing at least three individuals (Fig. 2 and Supplementary Table 3).

Locality and horizon. Near the base of the Lifua Member of the Manda Beds (Anisian based on biostratigraphical correlations with the *Cynognathus* subzone B assemblage zone of South Africa¹⁶), Ruhuhu Basin, Tanzania¹⁷; stratigraphically below the formerly oldest stem-avian *Asilisaurus kongwe*⁷ and other members of the typical faunal assemblage from the Manda Beds¹⁸ (Fig. 1).

Diagnosis. *T. rhadinus* differs from all other archosauriforms in the following combination of character states (*probable autapomorphy): neural canal openings of the anterior cervicals dorsoventrally elongated anteriorly, and mediolaterally elongated posteriorly*; anterior cervicals at least 1.5 times longer than anterior to middle trunk vertebrae; preacetabular process of the ilium arcs medially to create a distinct pocket on the medial surface; small concave ventral margin of the ischial peduncle of the ilium; long iliofibularis crest of the fibula (see Supplementary Information for differential diagnosis).

Description. The maxilla bears a prominent antorbital fossa that extends onto the posterior process and a medially extended palatal process that probably contacted its counterpart, both apomorphic conditions of Archosauria¹⁹. The single preserved tooth crown is labiolingually compressed, recurved and finely serrated on both margins. The frontal possesses a shallow, but prominent, supratemporal fossa, as in all early dinosaurs^{13,14}.

As in dinosauriforms, the anterior cervical vertebrae are substantially longer than the axis and the posterior cervical vertebrae; proportionally, they are among the longest of any Triassic avemetatarsalian (up to around 3.5 times longer than they are high). The anterior and middle cervical vertebrae possess posteriorly projecting epiphyses. The posterior cervical vertebrae have an extra articular surface between the parapophysis and diapophysis for three-headed ribs, similar to early crocodylids, *Yarasuchus* and some pseudosuchians^{19,20}. The elongated trunk vertebrae have well developed hypophene–hypoptrum articulations. *Teleocrater* possesses two sacral vertebrae, compared to three in *Nyasasaurus*²¹. The sacral ribs of the second sacral vertebra bear posterolaterally directed processes, which are known only in *Yarasuchus*, *Spondylosoma* and dinosauriforms among archosaurs (Supplementary Information). Osteoderms are not preserved and were probably absent.

The scapula has a distinct acromion process, as in most archosaurs and their close relatives (for example, proterochampsids²⁰). The posterior scapular margin bears a thin proximodistally oriented ridge, which is also present in silesaurids (Supplementary Information), and the glenoid fossa of the scapula is oriented mostly posteroventrally. The deltopectoral crest of the humerus is more than 30% of the length of the element, similar to *Nyasasaurus*²¹ and dinosaurs²², but unlike silesaurids and pterosaurs. From a single recovered metacarpal we infer that the hand was small relative to the rest of the forelimb.

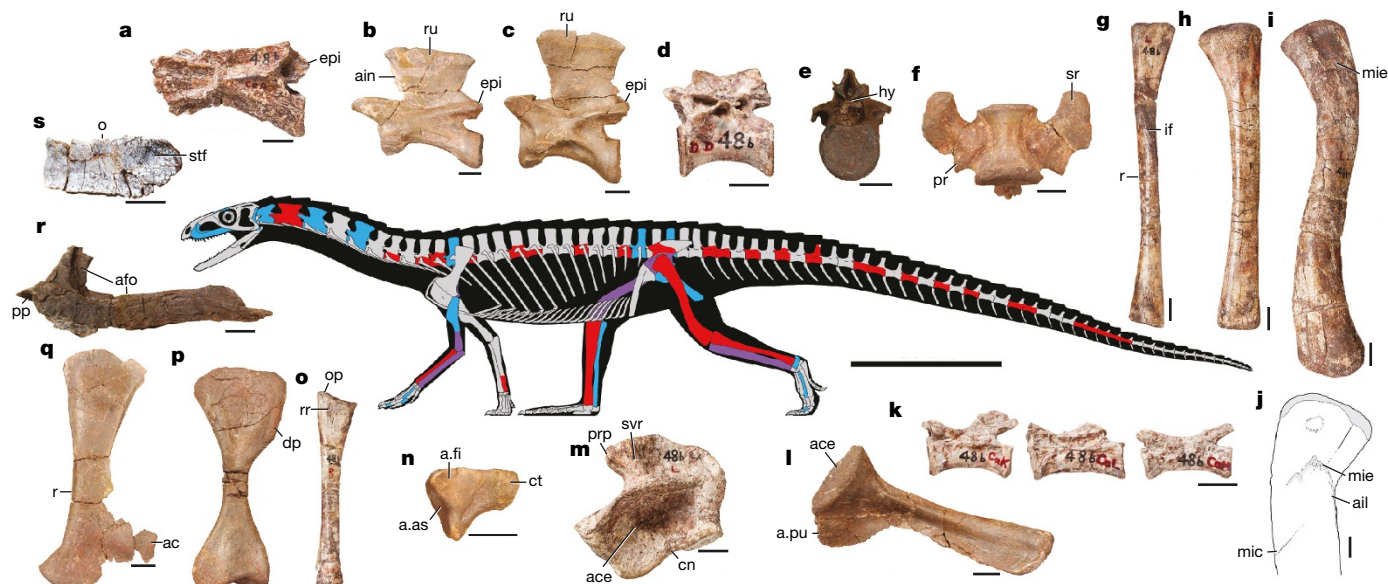


Figure 2 | Skeletal anatomy of *Teleocrater rhadinus* gen. et sp. nov.

a–c, Anterior and mid-cervical vertebrae (Natural History Museum, London, UK (NHMUK) PV R6795, National Museum of Tanzania, Dar es Salaam, Tanzania (NMT) RB505, NMT RB511). d–e, Middle and posterior trunk vertebrae (NHMUK PV R6795). f, Second sacral vertebra (NMT RB519). g, Left fibula (NHMUK PV R6795). h, Right tibia (NHMUK PV R6795). i, Left femur (NHMUK PV R6795). j, Muscle scars of right femur (NHMUK PV R6795). k, Posterior caudal vertebrae (NHMUK PV R6795). l, Left ischium (NMT RB479). m, Partial left ilium (NHMUK PV R6795). n, Right calcaneum (NMT RB490). o, Left ulna (NHMUK PV R6795). p, Left humerus (NMT RB476). q, Right scapula (NMT RB480). r, Left maxilla (NMT RB495). s, Right frontal (NMT RB496). Orientations: a–d, k, left lateral; e, posterior; f, ventral;

g, h, l, m, o, q, r, lateral; i, j, anterolateral; n, proximal; p, anterior; s, dorsal. Scale bars, a–s, 1 cm; skeleton, 25 cm. Red, holotype; blue, referred; purple, in holotype and referred; grey, unknown. a., articulates with; ac, acromion; ace, acetabulum; afo, antorbital fossa; ain, anteriorly inclined anterior margin of the neural spine; as, astragalus; cn, concave notch; ct, calcaneal tuber; dp, deltopectoral crest; epi, epiphyses; fi, fibula; hy, hypophene; if, M. iliofemoralis scar; lic, linea intermuscularis cranialis; mic, M. iliotochantericus caudalis scar; mie, M. iliofemoralis externus scar; o, orbital margin; op, olecranon process; pp, palatal process; pr, posterolateral process; prp, preacetabular process; pu, pubis; r, ridge; rr, radius ridge; ru, rugosity; sr, sacral rib; stf, supratemporal fossa; svr, subvertical ridge.

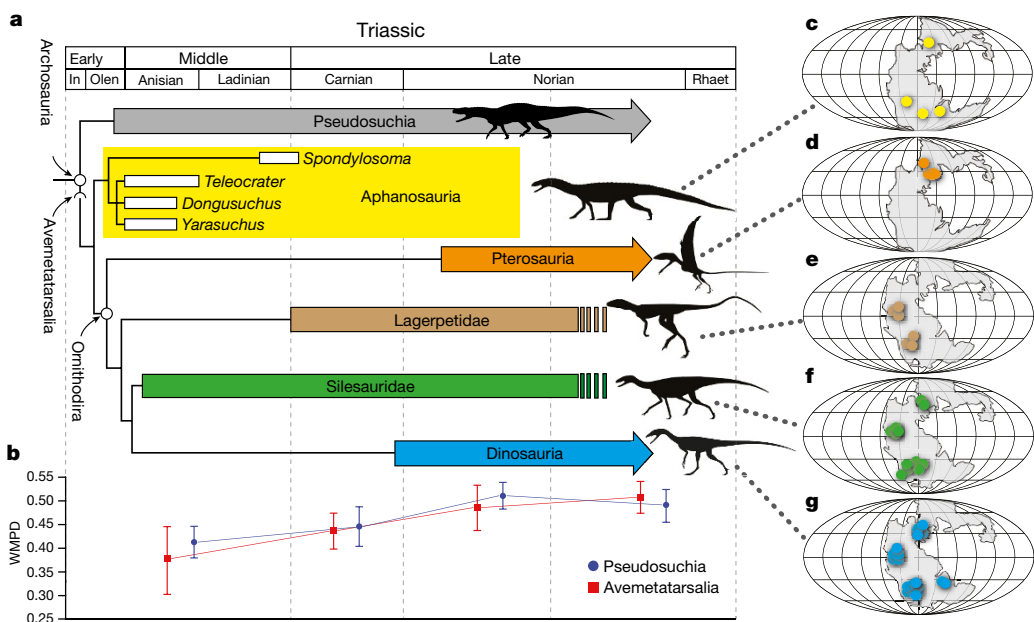


Figure 3 | Early evolution of avemetatarsalians. **a**, Interrelationships of Avemetatarsalia derived from two datasets^{19,20} (Supplementary Information). All clades except Aphanosaura have been collapsed for clarity. The lengths of the white bars indicate stratigraphic imprecision. In, Induan; Olen, Olenekian; Rhaet, Rhaetian. **b**, Plot of morphological disparity for Pseudosuchia (including Phytosaurs) and Avemetatarsalia for the duration of the Triassic period. Plots show weighted mean pairwise

The acetabulum of *Teleocrater* was closed, but a small concave notch on the ischial peduncle suggests a small perforation of the acetabulum, as in *Asilisaurus*⁷ and *Silesaurus*⁶. A distinct vertical crest extending dorsally from the supraacetabular rim separates a medially projecting preacetabular process from the rest of the ilium, similar to *Marasuchus*¹¹ and *Asilisaurus*⁷.

The proximal surface of the femur of *Teleocrater* has a deep longitudinal groove, and there is no anteromedial tuber (postero-medial tuber in ref. 20), unlike nearly all archosaurs^{19,20}. As in dinosauromorphs, a proximally placed M. iliofemoralis externus scar is present and connected to the anterior intermuscular line. However, in *Teleocrater* the M. iliofemoralis externus scar is well separated from the M. iliotrochantericus caudalis scar and lies in the plesiomorphic position present in early archosaurs and their close relatives¹⁹, as well as in *Dongusuchus* and *Yarasuchus* (Extended Data Fig. 1). The posterior surface of the distal medial condyle possesses a proximodistally oriented scar that is also present in dinosauromorphs (Supplementary Information). The tibia lacks a cnemial crest and any differentiation of its distal end, contrasting with proterochampsids and dinosauromorphs^{19,20}. The proximal half of the fibula has a long, twisted iliofibularis crest. The calcaneum bears the character states of a ‘crocodile-normal’ ankle configuration, a concave astragalar facet that permitted movement between the calcaneum and astragalus, as well as a taller than broad and posteriorly directed calcaneal tuber and a distinctly rounded fibular facet. Osteohistology of the *Teleocrater* humerus and fibula suggest sustained, elevated growth rates (Extended Data Fig. 2; Supplementary Information) similar to those of many ornithodirans^{21,23}.

Our phylogenetic analyses recovered *Teleocrater* in a clade containing *Yarasuchus*, *Dongusuchus* and *Spondyloma*. This previously unrecognized clade, named Aphanosaura herein, is resolved as the earliest diverging group on the avian stem lineage (Extended Data Figs 3, 4; Supplementary Information). The body plans of *Teleocrater* and other aphanosaurs demonstrate a previously undocumented transitional morphology between the common ancestor of archosaurs and dinosaurs and their closest relatives. Aphanosaurs were

dissimilarity (WMPD, see Methods). **c–g**, Geographical distributions of major subclades of avemetatarsalians during the Triassic. **c**, Aphanosaura. **d**, Pterosauria. **e**, Lagerpetidae. **f**, Silesauridae. **g**, Dinosauria. See Supplementary Table 5 for occurrences. Palaeogeographic maps were modified from <https://www2.nau.edu/rcb7/globaltext2.html>. Source map from Ron Blakey, copyright 2012 Colorado Plateau Geosystems Inc.

long-necked, non-cursorial and carnivorous, and so more like stem-archosaurs and pseudosuchians than later avemetatarsalians. *Teleocrater* confirms that several key character states of the ankle that together form the crocodile-normal configuration are plesiomorphic for both Archosauria and Avemetatarsalia. The distribution of ankle morphologies among early dinosauriforms is much more complex than previously appreciated, with crocodile-normal character states retained by the silesaurids *Lewisuchus* and *Asilisaurus*⁷, *Marasuchus*, and some early dinosaurs (Extended Data Fig. 5). This implies repeated evolution within Avemetatarsalia of the character states typical of the ‘advanced mesotarsal’ ankle configuration present in pterosaurs, lagerpetids and dinosaurs, although the functional implications of these convergent acquisitions require rigorous biomechanical evaluation (see Supplementary Information).

Several of the character states supporting Aphanosaura at the base of Avemetatarsalia were once thought to characterize only dinosaurs (for example, supratemporal fossa on the frontal²) or dinosauromorphs (for example, hypophene-hypantra in trunk vertebrae²), but *Teleocrater* demonstrates that these morphologies have a deeper history. Comparison of the hindlimb proportions (femur–tibia–longest metatarsal ratios) of early archosaurs and close relatives indicates that *Teleocrater* and silesaurids have proportions similar to those of stem-archosaurs and pseudosuchians (Extended Data Fig. 6), and that these proportions probably represent the ancestral avemetatarsalian condition. Lagerpetids, pterosaurs, and small- to medium-sized dinosaurs (for example, early ornithischians, coelophysoids) all lengthened the metatarsus relative to the femur and tibia, in association with increasingly cursorial adaptations²⁴. However, it is currently unclear how many times these hindlimb modifications evolved independently, given the complex distribution of character states among these taxa.

Aphanosaurs, like the earliest pseudosuchians^{25,26}, were widespread across Pangaea during the Middle Triassic, and the major subclades of avemetatarsalians (for example, Aphanosaura, Lagerpetidae, Silesauridae, Dinosauria) underwent repeated biogeographic expansions across Pangaea throughout the Middle and Late Triassic (Fig. 3). The discoveries of Aphanosaura and other specialized Triassic

avemetatarsalians call into question the hypothesis that pseudosuchians were more morphologically disparate than avemetatarsalians during the Triassic period^{27,28}. We estimated weighted mean pairwise disparity for Avemetatarsalia and Pseudosuchia using a data matrix including the new information presented here and, in contrast to previous analyses^{27,28}, found no significant difference in disparity between the clades for the entire dataset or for any individual time bin (Fig. 3).

Aphanosaurs, and other discoveries, demonstrate that early avemetatarsalians had much more complex biogeographic and evolutionary histories than previously appreciated. Analyses of dinosaur origins have usually assumed that their immediate ancestors resembled highly cursorial taxa such as *Marasuchus* and *Lagerpeton*. This assumption is challenged by the recognition of non-cursorial avemetatarsalian taxa such as aphanosaurs and silesaurids, indicating that current models of dinosaur origins are in need of revision.

Online Content Methods, along with any additional Extended Data display items and Source Data, are available in the online version of the paper; references unique to these sections appear only in the online paper.

Received 10 October 2016; accepted 28 February 2017.

Published online 12 April 2017.

1. Benton, M. J. & Clark, J. M. in *The Phylogeny and Classification of the Tetrapods. Volume 1: Amphibians, Reptiles, Birds. Systematics Association Special Volume 35A* (ed. Benton, M. J.) 295–338 (Clarendon, 1988).
2. Gauthier, J. Saurischian monophyly and the origin of birds. *Mem. Calif. Acad. Sci.* **8**, 1–55 (1986).
3. Sereno, P. C. Basal archosaurs: phylogenetic relationships and functional implications. *Soc. Vertebr. Paleontol. Mem.* **2**, 1–53 (1991).
4. Sereno, P. C. The evolution of dinosaurs. *Science* **284**, 2137–2147 (1999).
5. Dalla Vecchia, F. M. in *Anatomy, Phylogeny, and Palaeobiology of Early Archosaurs and their Kin Vol. 379* (eds Nesbitt, S. J., Desojo, J. B. & Irmis, R. B.) 119–155 (Geological Society, 2013).
6. Dzik, J. A beaked herbivorous archosaur with dinosaur affinities from the early Late Triassic of Poland. *J. Vertebr. Paleontol.* **23**, 556–574 (2003).
7. Nesbitt, S. J. et al. Ecologically distinct dinosaurian sister group shows early diversification of Ornithodira. *Nature* **464**, 95–98 (2010).
8. Benton, M. J. *Scleromochlus taylori* and the origin of dinosaurs and pterosaurs. *Phil. Trans. R. Soc. Lond. B* **354**, 1423–1446 (1999).
9. Benton, M. J. & Walker, A. D. *Saltopus*, a dinosauriform from the Upper Triassic of Scotland. *Earth Environ. Sci. Trans. R. Soc. Edinb.* **101**, 285–299 (2010).
10. Sereno, P. C. & Arcucci, A. B. Dinosaurian precursors from the Middle Triassic of Argentina: *Lagerpeton chanarensis*. *J. Vertebr. Paleontol.* **13**, 385–399 (1994).
11. Sereno, P. C. & Arcucci, A. B. Dinosaurian precursors from the Middle Triassic of Argentina: *Marasuchus lilloensis*, gen. nov. *J. Vertebr. Paleontol.* **14**, 53–73 (1994).
12. Bakker, R. T. & Galton, P. M. Dinosaur monophyly and a new class of vertebrates. *Nature* **248**, 168–172 (1974).
13. Brusatte, S. L. et al. The origin and early radiation of dinosaurs. *Earth Sci. Rev.* **101**, 68–100 (2010).
14. Langer, M. C., Ezcurra, M. D., Bittencourt, J. S. & Novas, F. E. The origin and early evolution of dinosaurs. *Biol. Rev. Camb. Philos. Soc.* **85**, 55–110 (2010).
15. Irmis, R. B. et al. A Late Triassic dinosauromorph assemblage from New Mexico and the rise of dinosaurs. *Science* **317**, 358–361 (2007).
16. Rubidge, B. S. Re-uniting lost continents – fossil reptiles from the ancient Karoo and their wanderlust. *S. Afr. J. Geol.* **108**, 135–172 (2005).

17. Wopfner, H. Tectonic and climatic events controlling deposition in Tanzanian Karoo basins. *J. Afr. Earth Sci.* **34**, 167–177 (2002).
18. Sidor, C. A. et al. Provincialization of terrestrial faunas following the end-Permian mass extinction. *Proc. Natl. Acad. Sci. USA* **110**, 8129–8133 (2013).
19. Nesbitt, S. J. The early evolution of archosaurs: relationships and the origin of major clades. *Bull. Am. Mus. Nat. Hist.* **352**, 1–292 (2011).
20. Ezcurra, M. D. The phylogenetic relationships of basal archosauromorphs, with an emphasis on the systematics of proterosuchian archosauriforms. *PeerJ* **4**, e1778 (2016).
21. Nesbitt, S. J., Barrett, P. M., Werning, S., Sidor, C. A. & Charig, A. J. The oldest dinosaur? A Middle Triassic dinosauriform from Tanzania. *Biol. Lett.* **9**, 20120949 (2012).
22. Langer, M. C. & Benton, M. J. Early dinosaurs: a phylogenetic study. *J. Syst. Palaeontol.* **4**, 309–358 (2006).
23. Padian, K., Horner, J. R. & de Ricqlès, A. Growth in small dinosaurs and pterosaurs: the evolution of archosaurian growth strategies. *J. Vertebr. Paleontol.* **24**, 555–571 (2004).
24. Kubo, T. & Kubo, M. O. Associated evolution of bipedality and cursoriality among Triassic archosaurs: a phylogenetically controlled evaluation. *Paleobiology* **38**, 474–485 (2012).
25. Butler, R. J. et al. The sail-backed reptile *Ctenosauroides* from the latest Early Triassic of Germany and the timing and biogeography of the early archosaur radiation. *PLoS One* **6**, e25693 (2011).
26. Butler, R. J. et al. New clade of enigmatic early archosaurs yields insights into early pseudosuchian phylogeny and the biogeography of the archosaur radiation. *BMC Evol. Biol.* **14**, 128 (2014).
27. Brusatte, S. L., Benton, M. J., Lloyd, G. T., Ruta, M. & Wang, S. C. Macroevolutionary patterns in the evolutionary radiation of archosaurs (Tetrapoda: Diapsida). *Earth Environ. Sci. Trans. R. Soc. Edinb.* **101**, 367–382 (2010).
28. Brusatte, S. L., Benton, M. J., Ruta, M. & Lloyd, G. T. Superiority, competition, and opportunism in the evolutionary radiation of dinosaurs. *Science* **321**, 1485–1488 (2008).

Supplementary Information is available in the online version of the paper.

Acknowledgements We acknowledge A. Tibaijuka for help with fieldwork logistics in Tanzania. Supported by National Geographic Society Research & Exploration grant (9606-14, S.J.N.), National Science Foundation EAR-1337569 (C.A.S.) and EAR-1337291 (K.D.A., S.J.N.), a Marie Curie Career Integration Grant (630123, R.J.B.), a National Geographic Society Young Explorers grant (9467-14 M.D.E.), and the Russian Government Program of Competitive Growth of Kazan Federal University and RFBR 14-04-00185, 17-04-00410 (A.G.S.). We thank S. Chapman, A. C. Milner, M. Lowe and S. Bandyopadhyay for access to specimens, S. Werning, G. Lloyd, R. Close and K. Padian for discussions, and H. Taylor for photographs of the holotype.

Author Contributions S.J.N., R.J.B., M.D.E. and P.M.B. designed the research project; C.A.S. and K.D.A. designed the field project; S.J.N., C.A.S., K.D.A., R.M.H.S. and M.R.S. conducted fieldwork; S.J.N., R.J.B., M.D.E., P.M.B., M.R.S. and A.J.C. described the material; S.J.N., M.D.E. and M.R.S. conducted the phylogenetic analyses; R.J.B. conducted disparity analyses; and S.J.N., R.J.B., M.D.E., P.M.B., M.R.S., K.D.A., R.M.H.S., C.A.S., G.N. and A.G.S. wrote the manuscript.

Author Information Reprints and permissions information is available at www.nature.com/reprints. The authors declare no competing financial interests. Readers are welcome to comment on the online version of the paper. Publisher's note: Springer Nature remains neutral with regard to jurisdictional claims in published maps and institutional affiliations. Correspondence and requests for materials should be addressed to S.J.N. (sjn2104@vt.edu).

Reviewer Information *Nature* thanks K. Padian and H.-D. Sues for their contribution to the peer review of this work.

METHODS

Systematic palaeontology. Aphanosuria clade nov.

Etymology. ‘Aphanes’; hidden or obscure (Greek) and ‘sauros’, for lizard (Greek).

Definition. The most inclusive clade containing *Teleocrater rhadinus* and *Yarasuchus deccanensis* Sen, 2005 but not *Passer domesticus* Linnaeus, 1758 or *Crocodylus niloticus* Laurenti, 1768.

Diagnosis. Aphanosuria differs from all other archosaurs in possessing the following unique combination of character states: elongate cervical vertebrae with epiphyses and anteriorly overhanging neural spines that have rugose lateral margins on their dorsal ends; elongated deltopectoral crest that is at least 35% the length of the humerus; wide distal end of the humerus; femur with a scar for the M. iliofemoralis externus near the proximal surface (homologous with the anterior trochanter in dinosauromorphs) that is separate from the scar for the M. iliobrachialis caudalis (homologous with the trochanteric shelf in dinosauromorphs), without an anteromedial tuber, and with a straight, deep groove in the proximal surface; calcaneal tuber taller than broad (see Supplementary Information).

Histology. We sampled two specimens, a partial right fibula consisting of the proximal and distal ends (NMT RB488; Extended Data Fig. 1) and a left humerus (NMT RB476; Extended Data Fig. 2). We sampled close to the midshaft for NMT RB488 by extracting a small piece located at the proximal-most preserved portion of the distal end; a small chip was removed from the midshaft of NMT RB476 (Extended Data Fig. 2). Taking advantage of natural cracks in both specimens, the target portions of the bones were removed by applying acetone to the surface followed by gentle pressure to remove the pieces. The pieces were embedded in a clear polyester resin (Castolite AP) under vacuum. The block of polyester resin was cut into 1 mm thick thin-sections using an Isomet 1000 saw (Buehler Inc.) equipped with a diamond wafering blade. The thin-sections were adhered to plastic slides using Aron Alpha (Type 201) cyanoacrylate. Both sections were then ground down using standard practices²⁹ to the point at which light could pass through the bone. The thin-sections were imaged with regular transmitted light (bright field) and a full wave retarder ($\lambda = 530$ nm) (Extended Data Fig. 2).

Phylogenetic analysis. The relationships of *T. rhadinus* were analysed using the two most comprehensive, and largely independent, datasets available for Triassic archosauromorphs^{19,20}. Both matrices were analysed under equally weighted parsimony using TNT 1.5 (refs 30, 31). A heuristic search with 100 replicates of Wagner trees (with a random addition sequence) followed by TBR branch-swapping (holding 10 trees per replicate) was performed. The best trees obtained from the replicates were subjected to a final round of TBR branch swapping. Zero-length branches in any of the recovered MPTs were collapsed. Decay indices (= Bremer support values) were calculated and a bootstrap resampling analysis, using 1,000 pseudoreplicates, was performed reporting both absolute and GC (that is, difference between the frequencies of recovery in pseudoreplicates of the original group and the most frequently recovered contradictory group) frequencies.

We added and deleted various taxa from the analysis of ref. 19 (deleted: *Archosaurus rossicus*, *Prestosuchus chiniquensis*, UFRGS 0156 T, UFRGS 152T, *Lewisuchus admixtus*, *Pseudolagosuchus gracilis* following ref. 19), based on more recent publications. We included new data (*Yonghesuchus sangbiensis* and character 413)²⁶ and excluded the wildcard taxa *Parringtonia gracilis* and *Erpetosuchus granti*²⁶. We added the holotype and referred femora of *Dongusuchus efremovi*, the hypodigm of *Y. deccanensis* (see Supplementary Information), and *Spondylosoma absconditum* (see Supplementary Information) for a total of 82 taxa. We did not include non-femoral elements from *D. efremovi* because of uncertainty of association and attribution to the taxon³². We employed a conservative scoring strategy for those newly added taxa that are represented by more than one specimen. We scored the holotype of *T. rhadinus* and all the referred material of the same taxon separately, and then combined them into a ‘*Teleocrater* combined’ terminal taxon. Similarly, we added information from a nearly complete, single skeleton of *A. kongwe* (NMT RB159) under the terminal taxon name ‘*Asilisaurus kongwe* skeleton’ and then combined those scores with the original holotype and referred material of *A. kongwe*⁷. Additionally, we scored the enigmatic taxon *Scleromochlus taylori* into the phylogeny (Extended Data Figs 7, 8 and see Supplementary Information). For the dataset from ref. 20, we used the taxon sampling of analysis 3 (ref. 20), with the addition of *S. absconditum*, *S. taylori* and *T. rhadinus*. For the latter two taxa we used the same strategy as for the dataset of ref. 19, and this resulted in a total of 86 taxa.

A few characters were modified and six new characters (414–419; Extended Data Fig. 10; see Supplementary Information) were added to the dataset of ref. 19 for a total of 419 characters. The following characters were ordered in the dataset of ref. 19: 32, 52, 121, 137, 139, 156, 168, 188, 223, 247, 258, 269, 271, 291, 297, 328, 356, 399 and 413. Five of the six new characters (601–605) added to the matrix

of ref. 19 were included in the dataset of ref. 20. The remaining character was not added because it was already included in the original version of this matrix. Fusion between the astragalus and calcaneum was added as an independent character (606) rather than as a state of character 532. Taxa with a fused astragalocalcaneum (for example, *Lagerpeton chanarensis*) were rescored as inapplicable for character 532. The modified data matrix contains a total of 606 characters. The following characters were ordered in the dataset of ref. 20: 1, 2, 7, 10, 17, 19, 20, 21, 28, 29, 36, 40, 42, 50, 54, 66, 71, 75, 76, 122, 127, 146, 153, 156, 157, 171, 176, 177, 187, 202, 221, 227, 263, 266, 279, 283, 324, 327, 331, 337, 345, 351, 352, 354, 361, 365, 370, 377, 379, 398, 410, 424, 430, 435, 446, 448, 454, 458, 460, 463, 472, 478, 482, 483, 489, 490, 504, 510, 516, 529, 537, 546, 552, 556, 557, 567, 569, 571, 574, 581, 582 and 588.

Disparity analysis. We estimated morphological disparity using the modified data matrix of ref. 19 (Fig. 3 and Extended Data Fig. 9). We chose this data matrix because its taxonomic and anatomical sampling of Triassic crown archosaurs is the most comprehensive available (whereas the data matrix of ref. 20 focuses primarily on stem-archosaurs). We supplemented this dataset by scoring a number of additional pseudosuchian and avemetatarsalian species, resulting in a final taxon list of 114 operational taxonomic units. From these data we estimated disparity for four time bins covering the Triassic archosaur radiation: (1) late Early Triassic–Middle Triassic; (2) Carnian; (3) early Norian; (4) late Norian–Rhaetian.

Disparity was estimated for three different groupings: (1) Avemetatarsalia; (2) Pseudosuchia without Phytosauria; (3) Pseudosuchia with Phytosauria (Fig. 3 and Extended Data Fig. 9). The latter grouping was chosen to reflect the traditional inclusion of Phytosauria within Pseudosuchia (as also recovered in the second of our phylogenetic analyses, based on the data matrix of ref. 20). Outgroup taxa were excluded from the data matrix before analysis. All ingroup taxa were assigned to one of the time bins. Nevertheless, *Machaeroprosopus pristinus* was assigned to both early Norian and late Norian–Rhaetian time bins, in order to ensure that phytosaur morphology was included in disparity calculations for all time bins in which the group is known to have been present.

Disparity was calculated as weighted mean pairwise dissimilarity^{33,34} in the R package Claddis³⁴. Results are presented in Supplementary Table 6. Bootstrapped 95% confidence intervals were calculated for weighted mean pairwise dissimilarities using 1,000 replicates. Disparity was calculated for each group in each time bin, as well as total disparity for each group, including all of its Triassic representatives.

Hindlimb disparity. In order to examine changes in hindlimb proportions among archosauriforms, we collected data on the lengths of the femur, tibia, and metatarsals III and IV, as well as the proximal widths of these two metatarsals, for 96 individuals representing 49 species, including four species of non-archosaurian archosauriforms, 17 pseudosuchian species, eight pterosaur species, 13 dinosaur species and seven species of non-dinosaurian, non-pterosaurian avemetatarsalians (including aphanosaurs, silesaurids, lagerpetids and *Marasuchus*) (Supplementary Table 7). Data were collected from the literature and directly from specimens.

For *T. rhadinus*, complete lengths of metatarsals III and IV were not available, although the proximal ends of both are preserved. In order to estimate the complete length of metatarsal III we conducted an ordinary least squares linear regression, using the proximal width of metatarsal III as the independent variable and metatarsal III length as the dependent variable (Supplementary Table 8). Data were log₁₀-transformed before analysis. The formula of the resultant regression model ($y = 0.634x + 1.09357; R^2 = 0.68, P = 1.285 \times 10^{-8}$) was used to estimate a length of 74.8 mm for metatarsal III of *T. rhadinus*. In order to visualize the hindlimb proportions for taxa in our dataset, we plotted them onto a ternary diagram using the R package ggtern³⁵ (Extended Data Fig. 6; Supplementary Information). Different symbols were used to plot the five major groups of archosauriforms covered by our data (see above), and the fill of the symbols was coloured according to femur length. Statistical analyses and plotting of data were conducted in R³⁶.

Further sources for silhouettes and reconstructions in Figs 1–3. In Fig. 1, taxa 1, 15, 18, 19 and 21 are from ref. 19, 2 from S. Hartman, 3, 4, 6, 20 and 24 (Public Domain Dedication 1.0) from Phylopic.org, 7 from S. Traver (Public Domain Dedication 1.0) from Phylopic.org. The skeletal reconstruction in Fig. 2 and the silhouettes of the pterosaur, silesaurid and dinosaur in Fig. 3 are by S. Hartman.

Data availability. All data (for example, R scripts, measurements used for the disparity analysis, phylogenetic datasets) that support the findings of this study are available at the Dryad repository at <http://dx.doi.org/10.5061/dryad.tj428>.

29. Lamm, E.-T. in *Bone Histology of Fossil Tetrapods: Advancing Methods, Analysis, and Interpretation* (eds Padian, K. & Lamm, E.-T.) 55–160 (Univ. California Press, 2013).
30. Goloboff, P. A., Farris, J. S. & Nixon, K. C. TNT: a free program for phylogenetic analysis. *Cladistics* **24**, 774–786 (2008).

31. Goloboff, P. A. & Catalano, S. A. TNT version 1.5, including a full implementation of phylogenetic morphometrics. *Cladistics* **32**, 221–238 (2016).
32. Niedzwiedzki, G., Sennikov, A. & Brusatte, S. L. The osteology and systematic position of *Dongusuchus efremovi* Sennikov, 1988 from the Anisian (Middle Triassic) of Russia. *Hist. Biol.* **28**, 550–570 (2016).
33. Close, R. A., Friedman, M., Lloyd, G. T. & Benson, R. B. Evidence for a mid-Jurassic adaptive radiation in mammals. *Curr. Biol.* **25**, 2137–2142 (2015).
34. Lloyd, G. T. Estimating morphological diversity and tempo with discrete character-taxon matrices: implementation, challenges, progress, and future directions. *Biol. J. Linn. Soc.* **118**, 131–151 (2016).
35. Hamilton, N. ggtern: an extension to ‘ggplot2’, for the creation of ternary diagrams. R package version 2.1.5. <https://CRAN.R-project.org/package=ggtern> (2016).
36. R Core Team. R: A language and environment for statistical computing. (R Foundation for Statistical Computing, Vienna, Austria, 2013).



Extended Data Figure 1 | See next page for caption.

Extended Data Figure 1 | Skeletal anatomy of the aphanosaurs

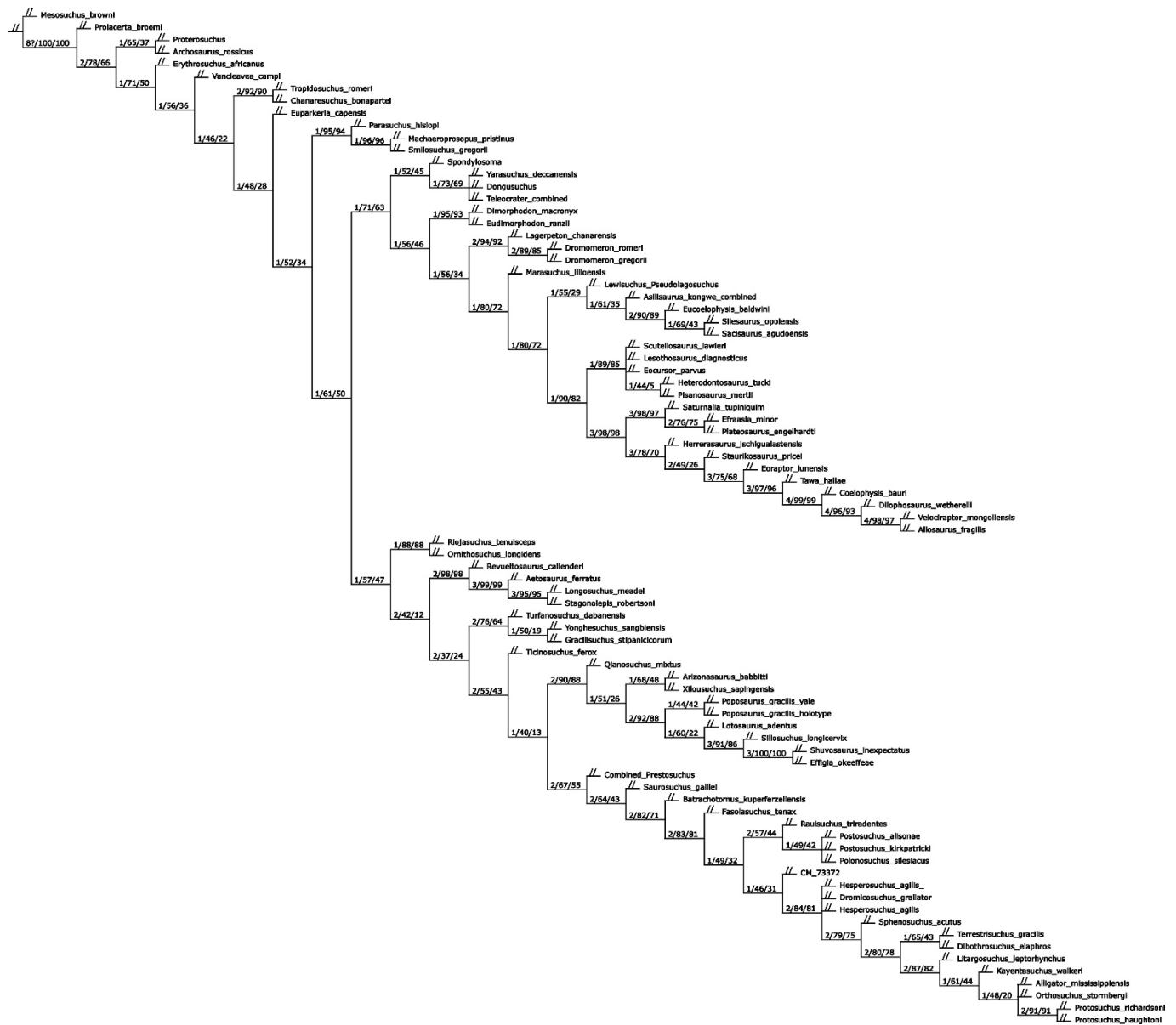
Dongusuchus efremovi, *Yarasuchus deccanensis* and *Spondylosoma absconditum*. **a, b**, *D. efremovi*. **c–t**, *Y. deccanensis*. **u–cc**, *S. absconditum*. **a, b**, Left holotype femur of *D. efremovi* (Borissiak Paleontological Institute of the Russian Academy of Sciences, Moscow, Russia (PIN) 952/15-1) in posteromedial (**a**) and anterolateral (**b**) views. **c–e**, Right partial femur of *Y. deccanensis* (Indian Statistical Institute, Kolkata, India (ISIR unnumbered) in posterolateral (**c**), proximal (**d**) and anterolateral (**e**) views. **f, g**, Left tibia of *Y. deccanensis* (ISIR 334) in posterior (**f**) and distal (**g**) views. **h, i**, Left calcaneum of *Y. deccanensis* (ISIR unnumbered) in proximal (**h**) and lateral (**i**) views. **j**, Second sacral vertebra of *Y. deccanensis* (ISIR BIA 45/43) in ventral view. **k**, Right ischium of *Y. deccanensis* (ISIR 334) in ventrolateral view. **l, m**, Posterior cervical vertebrae of *Y. deccanensis* (ISIR BIA 45/43) in posterior (**l**) and right lateral (**m**) views. **n, o**, Right humerus of *Y. deccanensis* (ISIR 334 53) in anterior (**n**) and posterior (**o**) views. **p**, Right ulna of *Y. deccanensis* (ISIR 334) in anterior view. **q**, Trunk vertebra of *Y. deccanensis* (ISIR BIA

45/43) in left lateral view. **r, s**, Posterior cervical vertebrae of *Y. deccanensis* (ISIR BIA 45/43) in posterior (**r**) and right lateral (**s**) views. **t**, Triple-headed rib of *Y. deccanensis* (ISIR BIA 45) in anterior view. **u, x**, Original condition (**u**) of a cervical vertebra (from Huene 1942) of *S. absconditum* (Paläontologische Sammlung der Universität Tübingen, Tübingen, Germany (GPIT) 479/30) compared to that of the current condition (**x**). **v, w, y**, Original condition of a more posterior cervical vertebra of *S. absconditum* (from Huene 1942) in left lateral (**v**) and anterior (**w**) views compared to that of the current condition of the same vertebra in left lateral (**y**) view. **z**, Trunk vertebra of *S. absconditum* in posterior view. **aa**, Second sacral vertebra of *S. absconditum* in dorsal view. **bb, cc**, Right scapula of *S. absconditum* in lateral (**bb**) and posterior (**cc**) views. **a.**, articulates with; **ain**, anteriorly inclined anterior margin of the neural spine; **as**, astragalus; **ct**, calcaneal tuber; **dp**, deltopectoral crest; **fi**, fibula; **hy**, hypophene; **mic**, *M. iliotochantericus caudalis* scar; **mie**, *M. iliofemoralis externus* scar; **pr**, posterolateral; **r**, ridge. Scale bars, 1 cm. Outline of Africa and Tanzania obtained from Google Maps.



Extended Data Figure 2 | Histological sections of the limb bones of *T. rhadinus* gen. et sp. nov. **a**, Right fibula (NMT RB 488) in lateral (left) and medial (right) views. **b**, Photo of the histological section of the fibula (NMT RB 488) in regular transmitted light (bright field) (1 plane polarizer). **c**, Photo of the same section as in **b** using a full wave retarder ($\lambda = 530$ nm). **d**, Left humerus (NMT RB476) in posterior (left) and

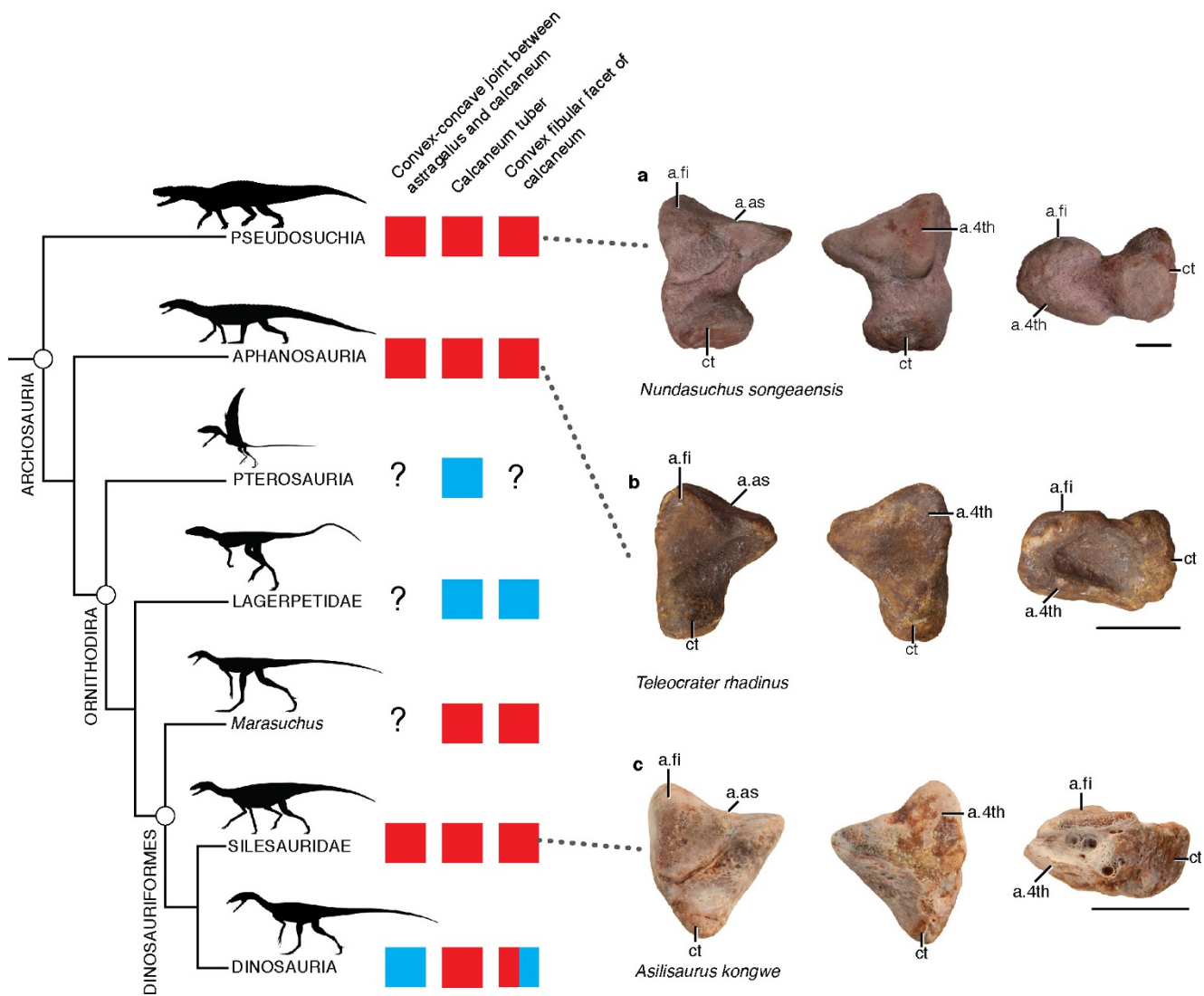
anterior (right) views. **e**, Photo of a partial histological section of the humerus (NMT RB476) in regular transmitted light (bright field) (1 plane polarizer). **f**, Photo of the same section as in **e** using a full wave retarder ($\lambda = 530$ nm). Scale bars, 1 mm. Arrows in **a**, **d** indicate where each element was sampled. Arrows in **b**, **c**, **e**, **f** indicate growth marks in the outer cortex.



Extended Data Figure 3 | The relationships of *T. rhadinus* gen. et sp. nov. among archosauriforms from the Nesbitt dataset. The dataset used has been described in ref. 19. Strict consensus of 36 most parsimonious trees (tree length = 1,374; consistency index = 0.3559; retention index = 0.7807). Bremer support values (first), absolute (second), and GC (third) bootstrap frequencies presented at each branch.

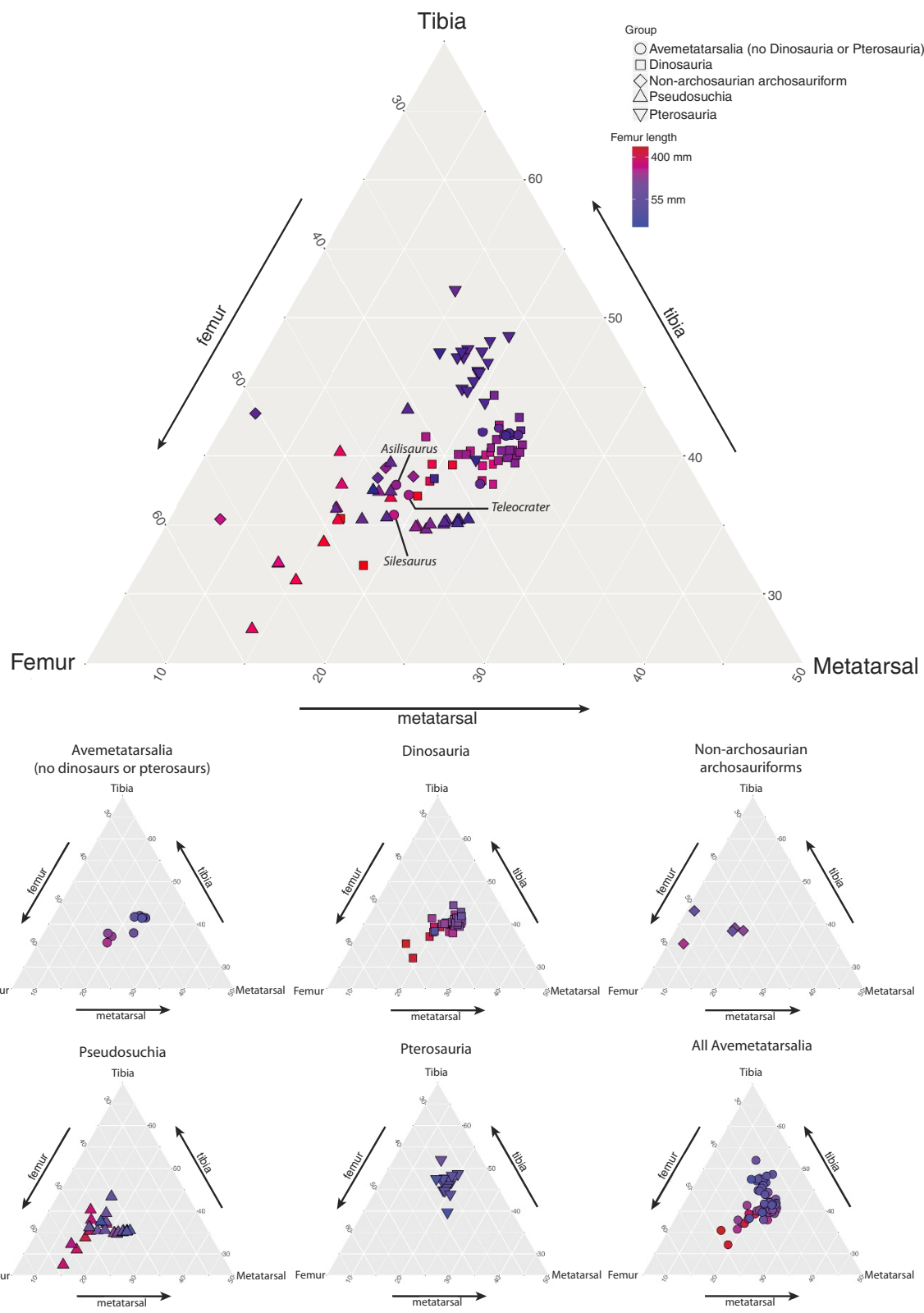


Extended Data Figure 4 | The relationships of *Teleocrater rhadinus* gen. et sp. nov. among archosauriforms from the Ezcurra dataset. The dataset used has been described in ref. 20. Strict consensus of four most parsimonious trees (tree length = 2,684; consistency index = 0.2955; retention index = 0.6284). Bremer support values (first), absolute (second), and GC (third) bootstrap frequencies presented at each branch.

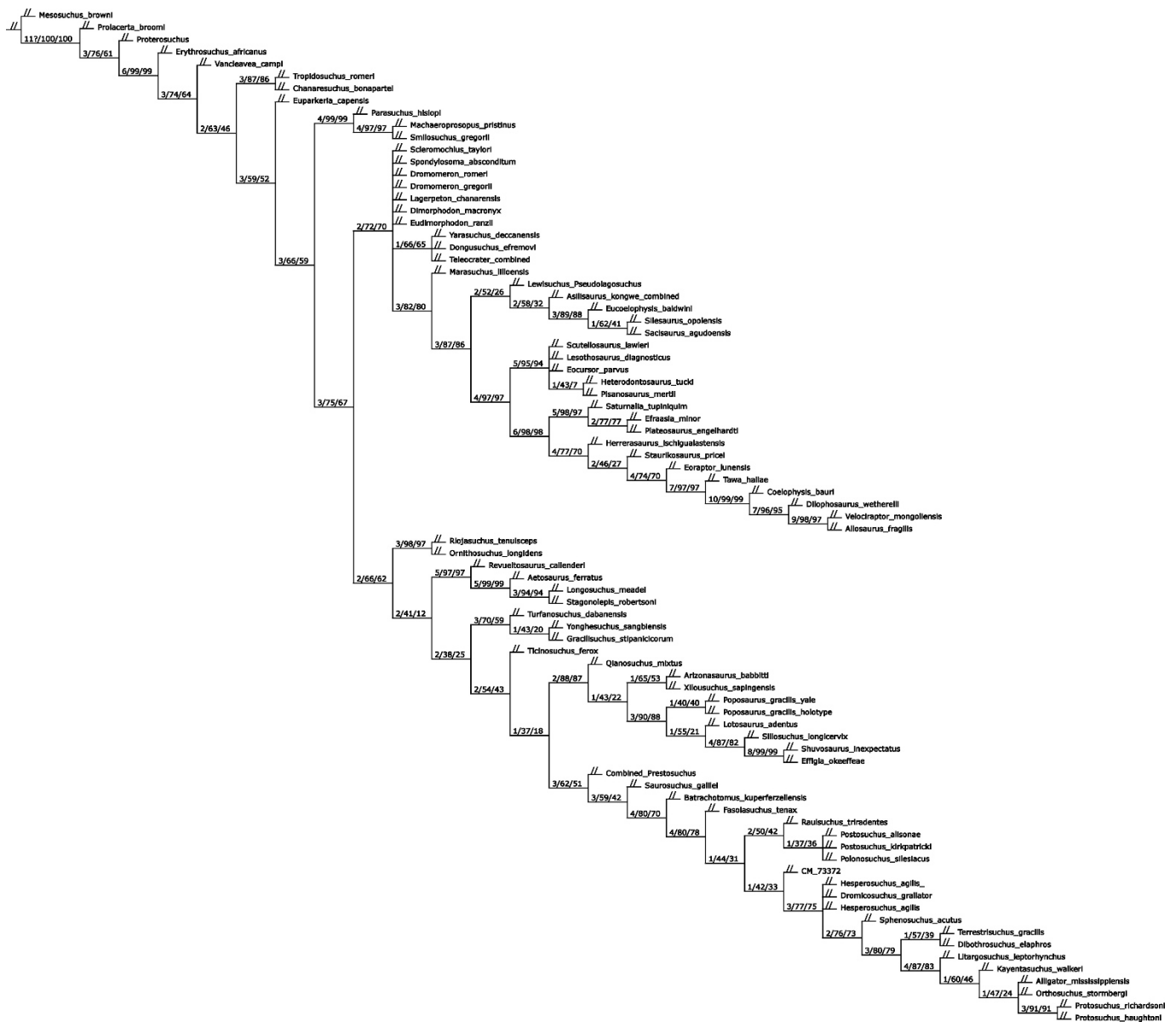


Extended Data Figure 5 | Phylogeny of early Avemetatarsalia illustrating the character distributions of the components of the crocodile-normal ankle configuration and showing that this ankle type was plesiomorphic for Archosauria, Avemetatarsalia, and possible less inclusive clades within Avemetatarsalia (for example, Dinosauriformes). **a**, Left calcaneum of the pseudosuchian *Nundasuchus songaeensis* (NMT RB48). **b**, Right calcaneum of the aphanosaur

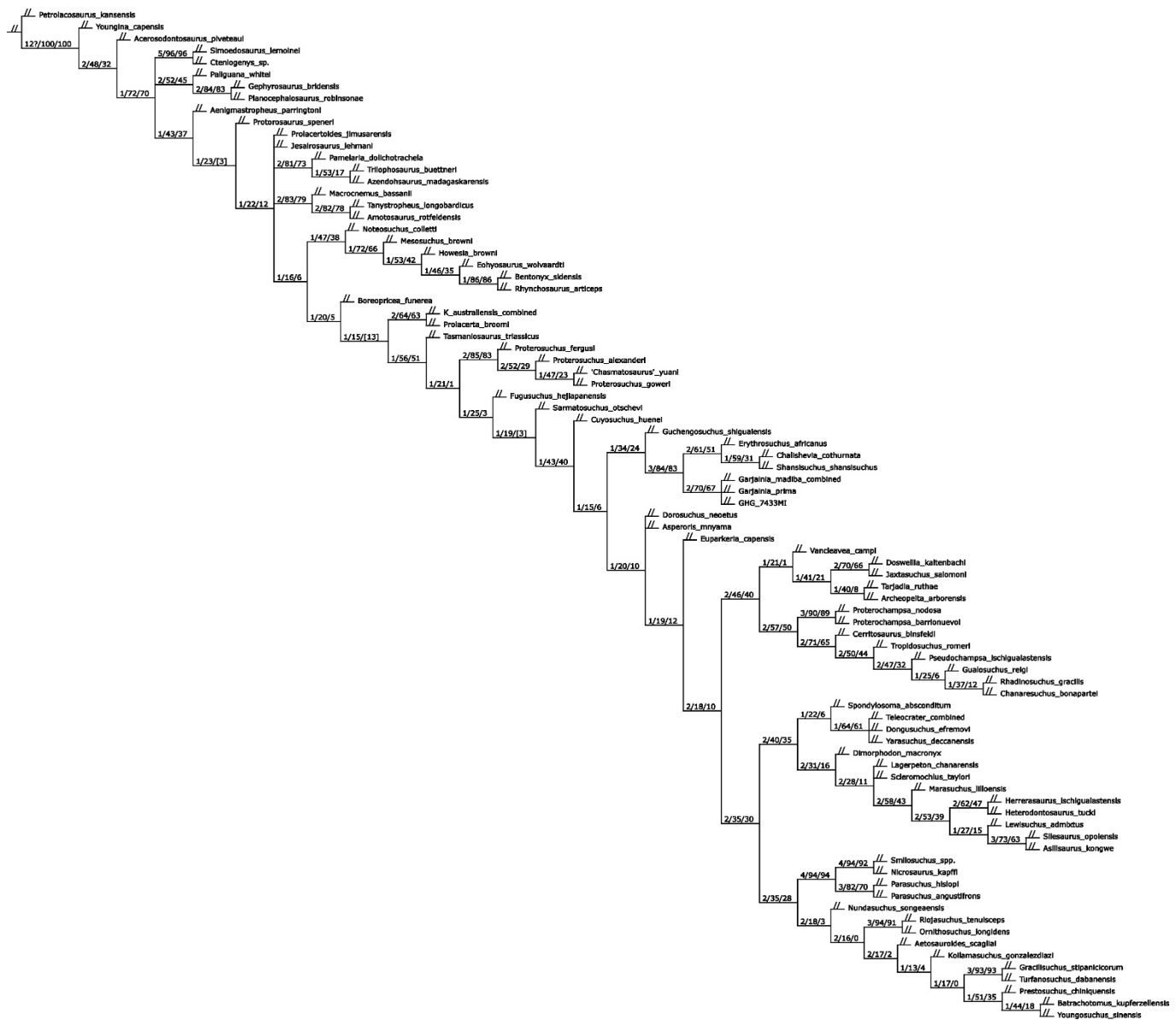
T. rhadinus gen. et sp. nov. (reversed) (NMT RB490). **c**, Left calcaneum of the dinosauriform silesaurid *A. kongwe* (NMT RB159). Proximal view (left), distal view (middle) and lateral view (right). Scale bars, 1 cm. red, character state present; blue, character state absent; red and blue, basal condition could be either; ?, unknown condition. See Fig. 3 for silhouette sources. 4th, fourth tarsal; a., articulates with; as, astragalus; ct, calcaneal tuber; fi, fibula.



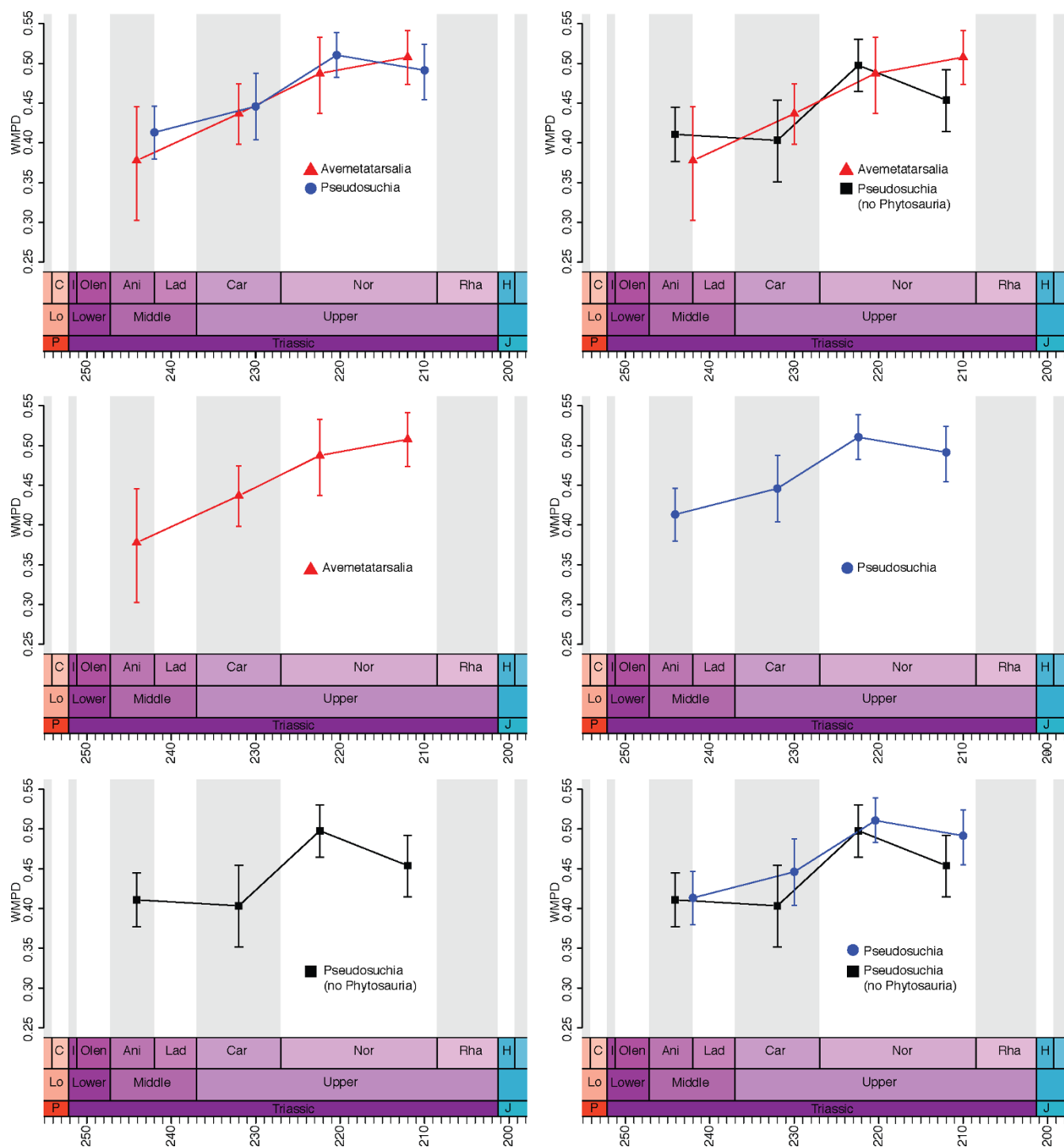
Extended Data Figure 6 | Ternary diagrams of measurements of the hindlimb elements (femur, tibia and longest metatarsal) of archosauriforms.
Colour of data points relates to femoral length.



Extended Data Figure 7 | The relationships of *S. taylori* among archosauriforms from the Nesbitt dataset. The dataset used has been described in ref. 19. Strict consensus of 792 most parsimonious trees (tree length = 1,378; consistency index = 0.3549; retention index = 0.7803) (see Supplementary Information). Bremer support values (first), absolute (second), and GC (third) bootstrap frequencies presented at each branch.



Extended Data Figure 8 | The relationships of *S. taylori* among archosauriforms from the Ezcurra dataset. The dataset used has been described in ref. 20. Strict consensus of four most parsimonious trees (tree length = 2,693; consistency index = 0.2945; retention index = 0.6280) (see Supplementary Information). Bremer support values (first), absolute (second), and GC (third) bootstrap frequencies presented at each branch.



Extended Data Figure 9 | Disparity estimates for major archosaur groups and time intervals (weighted mean pairwise dissimilarity (WMPD)).
 Ani, Anisian; C, Changhsingian; Car, Carnian; H, Hettangian; I, Induan; J, Jurassic; Lad, Ladinian; Lo, Lopingian; Nor, Norian; Olen, Olenekian; P, Permian; Rha, Rhaetian.



Extended Data Figure 10 | New character illustrations for the phylogenetic analysis. See Supplementary Information.

a–c, Archosaurian iliac comparisons for character 414 in the modified dataset of ref. 19. **a**, Left ilium of *Teleocrater rhadinus* (NHMUK PV R6795) in lateral view. **b**, Right ilium of *Asilisaurus kongwe* (NMT RB159) in lateral view. **c**, Left ilium of *Batrachotomus kupferzellensis* (Staatliches Museum für Naturkunde Stuttgart (SMNS) 80273) in lateral view. **d–g**, Avemetatarsalian fibula comparisons for character 415 in the modified dataset of ref. 19. **d**, **e**, Left fibula of *T. rhadinus* (NHMUK PV R6795) in lateral (**d**) and posterior (**e**) views. **f**, **g**, Left fibula of *A. kongwe* (NMT RB159) in lateral (**f**) and posterior (**g**) views. Arrows highlight the posterior ridge, character 415 state 1. **h**, **i**, Archosauriform femoral

comparisons for character 417 in the modified dataset of ref. 19. **h**, Right femur of *Erythrosuchus africanus* (NHMUK PV R3592) in ventral view. **i**, Right femur of *T. rhadinus* (NHMUK PV R6795) in posteromedial view. White dotted regions highlight character 417, state 1. **j–m**, Avemetatarsalian second primordial sacral comparisons for character 416 in the modified dataset of ref. 19. **j**, **k**, Second primordial sacral vertebra of *T. rhadinus* (NMT RB519) in ventral (**j**) and posterior (**k**) views. **l**, **m**, The second primordial sacral vertebra of *A. kongwe* (NMT RB159) in ventral (**l**) and dorsal (**m**) views. Arrows highlight the posterior process of the sacral rib, character 416, state 1. Scale bars, 1 cm (**a–g**, **i–m**) and 5 cm (**h**).